JMEPEG (2021) 30:4946–4956
https://doi.org/10.1007/s11665-021-05566-x

1059-9495/$19.00

Mechanical Reliability and In Vitro Bioactivity of 3D-Printed Porous Polylactic Acid-Hydroxyapatite Scaffold

Chander Prakash, Gurmider Singh, Sunpreet Singh, W.L. Linda, H.Y. Zheng, Seeram Ramakrishna, and Roger Narayan

Submitted: 13 November 2020 / Revised: 30 January 2021 / Accepted: 6 February 2021 / Published online: 4 March 2021

The study aimed to investigate the mechanical reliability and in vitro bioactivity of the three-dimensional (3D) printed hydroxyapatite (HA) reinforced polylactic acid (PLA) porous scaffolds. The experiments have been performed to study the effect of HA wt.% in PLA matrix, infill density, and post-printing thermal-stimulus on the flexural and compressive strength. Next to this, the best combination of input parameters, in-response of the observed mechanical properties, was determined to print the test specimens for the analysis of reliability, through Weibull distribution. Further, the fracture morphology of the developed PLA/HA porous scaffolds has been investigated, using scanning electron microscopy, to observe the involved fracture mechanism. Moreover, the in vitro cell-culture with osteoblastic bone marrow mesenchymal stem cells-lines has been studied after 1, 3, and 7 days of seeding. The results of the study highlighted that the processing parameters have a strong impact on the mechanical properties of the 3D printed porous scaffolds. Further, the in vitro analysis showed excellent growth, proliferation, and differentiation of osteoplastic cells. Along with these, the result of the Weibull distribution advocated that the printed porous scaffolds are mechanically reliable. Overall, the present study unequivocally advocates that the 3D printed PLA/HA scaffold can be used for potential tissue engineering and biomedical applications.

Keywords 3D printing, hydroxyapatite, in vitro bioactivity, mechanical properties, polylactic acid, scaffolds, Weibull distribution

1. Introduction

Recently, the biomedical polymers have been exhibited great potential in biomedical industry as an active intelligent property (Ref 1, 2). Some of the biomedical polymers, such as polylactic acid (PLA), can recover their original geometry after exposed to external stimuli: such as pressure, thermal, light, electric, and magnetic filled. The source of such polymers is limited as some of them are natural biological materials and some of them are artificial composites (Ref 3, 4). Further, PLA is a biodegradable polymer that has been extensively used for biomedical applications (Ref 5). However, the major drawback of PLA is the lack of bioactivity that does not help in the osseointegration process when implant in human body (Ref 6, 7). To enhance the bioactivity of PLA, bioactive materials for instance graphene, Fe_3O_4, hydroxyapatite (HA), chitosan, etc. can be added as reinforcements (Ref 8). The reinforcement of these elements not only improves the bioactivity but also enhances the strength and stiffness of the matrix. As observed, the processing of PLA with bio-ceramics is quite difficult and researchers are actively engaged in developing a new innovative technique to process and fabricate shape-memory materials based on these composites (Ref 9–12). In the case of three-dimensional (3D) printing, the development of reinforced PLA systems, especially for biomedical application, is not only easy but uniform too (Ref 13), as this has been executed through preliminary mixing of PLA matrix and reinforcement while fabricating feedstock filament. Indeed, the 3D printing of such systems presents promising merits for biomedical scaffolds, for instance, it can generate complex 3D contours, porous architecture, and co-culture of multiple cells and incorporate growth factors (Ref 14). However, critical care is advisable for 3D printing of biomaterial through the use of a sterile environment for fabrication, architectural design, and maintaining compositions to target sophistication (Ref 15, 16). It has been reported that 15 wt.% of HA in the PLA matrix exhibited 98% shape memory effect (SME) that may be used for self-fitting as an alternative of implants for small bone defects (Ref 17-20). HA is quickly absorbed into the human body, while at the same time the body is no wiser than the invasion of a foreign body. Maybe the most fascinating function is that HA can bind to indistinguishable bone-forming unions and most suitable for

This invited article is part of a special topical focus in the *Journal of Materials Engineering and Performance* on Additive Manufacturing. The issue was organized by Dr. William Frazier, Pilgrim Consulting, LLC; Mr. Rick Russell, NASA; Dr. Yan Lu, NIST; Dr. Brandon D. Ribic, America Makes; and Caroline Vail, NSWC Carderock.

Chander Prakash, School of Mechanical Engineering, Lovely Professional University, Phagwara, Punjab 144411, India; **Gurmider Singh**, School of Mechanical and Materials Engineering, University College Dublin, Dublin, Ireland; **Sunpreet Singh** and **Seeram Ramakrishna**, Department of Mechanical Engineering, National University of Singapore, Singapore, Singapore; **W.L. Linda** and **H.Y. Zheng**, Department of Mechanical Engineering, Shandong University of Technology, Zibo, China; **Roger Narayan**, Biomedical Engineering, University of North Caroline, Chapel Hill. Contact e-mail: snprt.singh@gmail.com.

the fabrication of composite scaffolds. Thermodynamically, HA is the most stable compound for physiologically stable calcium phosphate in temperature, pH and body fluid composition. The four-dimensional (4D) capabilities of SMP are greatly affected by the 3D printing process parameters such as extrusion temperature and scanning speed (Ref 21). The 3D printed component having SME with lightweight structure may be used for self-shaping, self-folding, and self-unfolding performances of biomedical scaffolds/implants (Ref 22, 23). There are many specific applications of shape memory effect in the biomedical fields such as for wound closure by SMP suture materials, for opening of blocked vessels by stents, for the fixation of tissues or medical devices during surgery, microgripper with jaws of laser-activated SMP that can release devices intravasularly after positioning by catheter, SMP device that unfolds in the stomach and thus reduces the volume of the stomach for weight reduction of overweight patients, etc. Plenty of research work, on advanced 4D medical applications of such polymers/polymer composites, have been reported in the literature, as listed in Table 1.

After devolving 3D printed parts, most of the researchers are working on the optimization of the input process parameters to develop mechanical-tuned parts and analyzing their properties, but failure probability or reliability analysis of the mechanical properties of the prints is missing. Farzadi et al. (Ref 39) developed a calcium/sulfate-based porous scaffold for bone tissue engineering and studied the effect of layer printing delay on compressive strength and dimensional accuracy of printed porous prototypes. The *Weibull* analysis was performed to determine the reliability of printed scaffolds and results revealed the samples printed using 300 ms delay have high reliability and have a higher impact on the fracture mechanism during compression loads. Castilho et al. optimized the design topology to maximize the compressive strength of 3D printed phosphoric diluted α/β-tri-calcium phosphate scaffold and studied the reliability of the same. The reliability of scaffold based on compressive strength is not compromised and favorable for the biomedical applications (Ref 40, 41). Similarly, in (Ref 42) a new concept has been demonstrated for developing Sr-substituted Mg-based biodegradable scaffolds using powder-based 3D printing and studied the reliability of scaffold as a function of compressive strength, bending strength, and tensile strength.

The extensive analysis of mechanical properties revealed that the *Weibull* modulus is not compromised to any extent in as-fabricated scaffolds and exhibit higher *Weibull* modulus in compression compared to other scaffold compositions (Ref 43). The failure probability of 3D printed tri-calcium phosphate powder scaffolds was studied using *Weibull* analysis and it was found that all scaffolds are reliable and less probability of failure. Lu et al. (Ref 44) studied the flexural strength reliability of Yttria-stabilized tetragonal zirconia poly-crystal implants fabricated by additive manufacturing and subtractive manufacturing techniques using *Weibull* analysis. The *Weibull* modulus of additive-manufactured implants was lower than that of subtractive-manufactured. Castilho et al. (Ref 45) analyzed the strength of 3D printed porous calcium phosphate using a statistical *Weibull* approach, and the dependence of the compressive strength on the porosity was discussed.

From the literature, it has been ascertained that PLA reinforced with HA is an excellent material combination for the preparation of porous scaffold structures. Some of the literature also explains the tendency of PLA-HA combination as smart material with remarkable shape memory effects. Some of the key challenges associated with biomedical implants lie in achieving reliable mechanical properties, designed to satisfy functional requirements as scaffolds. The use of Weibull distribution, for understanding the reliability of the printed scaffolds in the context of mechanical characteristics, has already well documented in the literature. However, this paper presents the first of its kind application of Weibull distribution on analyzing the mechanical reliability of 3D printed PLA/HA composites with different parametric study, along with in vitro cell-culture analysis. This method of 3D printing with analysis could be used to fabricate complex and customized implants. The step-to-step methodology adopted in this work is shown in Fig. 1.

2. Materials and Methods

2.1 Stage 1

This stage was comprised of two tasks: (1) development of *in-house* PLA/HA-based feedstock filament and (2) printing of test specimens, using fused filament fabrication (FFF) filament, with *in-house* developed feedstock filaments. In the former

Table 1 List of innovative medical applications of 4D printed thermoplastics

Feedstock	Technology	Key 4D application(s)
Styrene-b-(ethylene-cobutylene)-b-styrene, polyethylene wax, and low density	Fused Filament Fabrication (FFF)	Flexible electronics (Ref 24)
DiAPLEX MM-4520 and Tecoflex EG-72D	FFF	Electronic devices (Ref 25)
Polyurethane MM4520	FFF	Stent (Ref 26)
Acrylate-based photosensitive resins	Digital Light Processing	Photosensitive part fabrication (Ref 27)
Photopolymer	Stereolithography (SLA)	Stents (Ref 28-30)
Liquid crystal elastomers	Inkjet printing	Miura-origami structure (Ref 31)
Polyurethane	FFF	Self-bending gripers (Ref 32, 33)
Ionomeric thermoplastic and Zn-neutralized poly(ethylene-co-methacrylic acid)	FFF	Folded structures (Ref 34)
Polyamide	FFF	Actuators (Ref 35)
PLA	FFF	Smart structure (Ref 36, 37)
Polypropylene/nylon 6	FFF	Actuators (Ref 38)

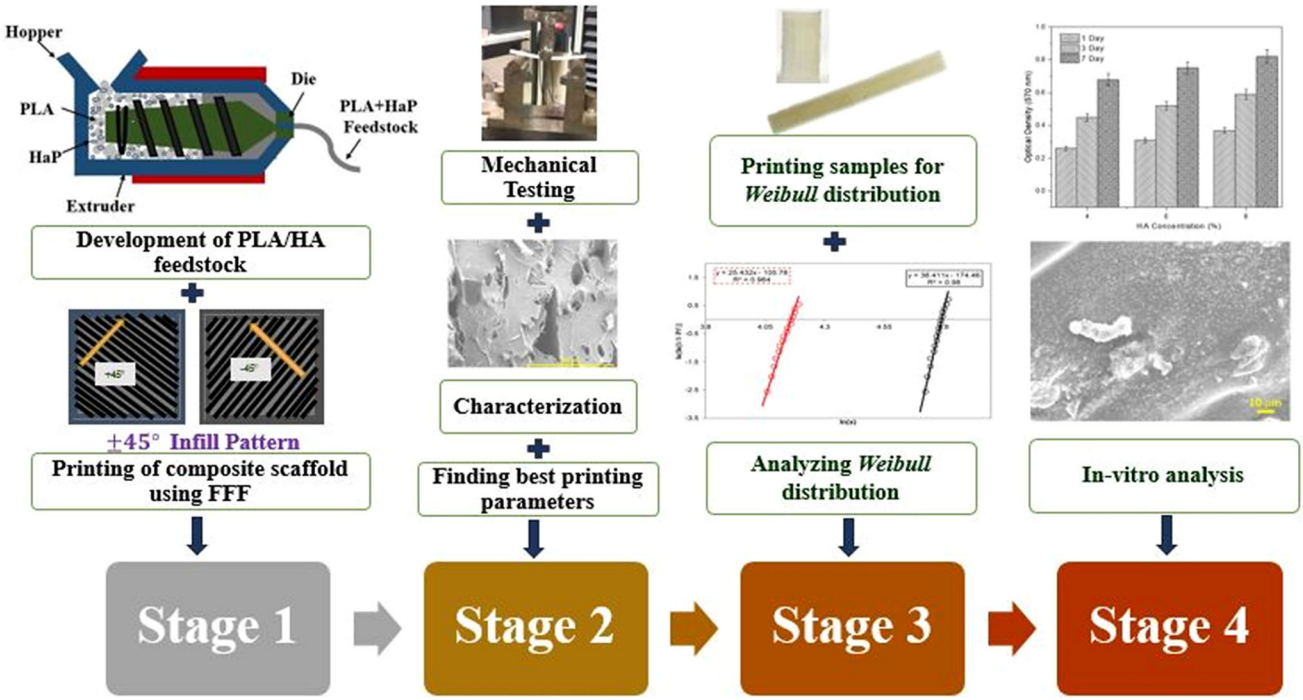

Fig. 1 Methodology of the present work

task, polylactic acid (PLA) granules containing 95% L-la, 95% L-lactide, and 5% meso-lactide were, selected as a polymer matrix, procured from Punjab Polymers (Ludhiana, India). The polydispersity index (PDI), molecular weight (M_w), and glass transition (T_g) temperature of PLA granules were $< 1.9M_w$/Mn, 1.6 × 105 (g/mole), and 58–60 °C, respectively. The granular consisted of cylindrical shapes was of an average length of 2 mm and a diameter of 1.5 mm. The reinforcement, hydroxyapatite (HA), was procured from a local vendor in the form fine powders of 0.15 µm average diameter. Both polymer matrix and HA powders were dried in a vacuum oven at 70 °C and 110 °C, respectively, for overnight to remove the moisture. Thereafter, HA powder was loaded in PLA matrix in three different proportions of 4, 6, and 8 wt.% For this, ball milling of PLA/HA mixtures was performed in Cryomill (Make: RETSZH, USA) for 4 number of cycles and dwelling time of 1 min. Finally, the development of the feedstock filaments for FFF system was carried out by using a twin-screw compounder (Make: MINI-HAAKE, Germany), and this resulted into three different filaments (with 4, 6, and 8 wt.% loading of HA), namely F1, F2, and F3, respectively, of an average diameter of 1.75 ± 0.05 mm. It should be noted that the three filaments were fabricated at 170 °C barrel temperature, 180 °C die temperature, and 50 rpm of the screw. In the task #2 of the first stage, the prepared feedstock filaments were used to print test specimens for mechanical (flexural (ASTM D790-10 type IV), tensile (ASTM D638 type IV), and compression (ASTM D695)) and in vitro analysis. For printing, a commercial FFF printer (Make: Divide by Zero, India) was used and printing was carried out at three different levels of infill percentage (20, 60, and 100%). Further, other printing parameters of FFF were considered static (35 mm/s infill speed, three outer perimeters, 195 °C printing temperature, 80 °C bed temperature, horizontal build orientation, ± 45° raster angle, and 0.2 mm extrusion nozzle diameter). The samples were, finally, heat-treated in an electric air convection heater at 60, 65, and 70 °C under a heating rate of 5 °C/min for 10 min.

The thermal-stimulus of as-printed porous scaffolds was carried out to enhance the interlayer adhesion of the printed specimens. Further, the glass transition (T_g) temperature of PLA is found in the range of 58–60 °C (ascertained by differential scanning calorimetry), thus, the range of thermal-stimulus temperature has been selected in the range of T_g temperature (Ref 36). Table 2 shows the range of printed samples and their settings. The as-fabricated scaffolds were investigated for the morphological analysis, refer to Fig. 2. Figure 2(a) shows the PLA scaffolds without HA and a smooth surface has been observed. On the other hand, when HA was loaded in PLA, a crystal-like structure was observed which conferred that HA was reinforced in PLA matrix, refer Fig. 2(b–d) shows the HA loaded PLA scaffolds surface. It can be seen that HA was uniformly reinforced in PLA matrix and different microstructure was observed as compared with PLA scaffolds. The structural porosity can also be observed.

2.2 Stage 2

In stage 2, mechanical testing of the printed PLA/HA scaffolds has been carried out for the flexural strength (FS) and compression strength (CS). All the tests were carried out on Universal Testing Machine. Figure 3 shows the fixture arrangements of flexural and compressive testing. The following equations were used to calculate the FS:

$$\sigma_f = \frac{3 \times F \times l}{2 \times b \times d^2}, \varepsilon_f = \frac{6 \times D \times d}{l^2}, \quad \text{(Eq 1)}$$

where σ_f and ε_f are flexural stress and strain, F and l are applied load and span length, b and d are samples width and thickness. All the results were provided as the average values of three measurements and standard deviations. Further, for analyzing the fractured surfaces, scanning electron microscopy

Table 2 Printed samples: parametric range and setting

wt.% of HA in PLA matrix	Infill density, %	Annealing temperature, °C
4	20	60
6	60	65
8	100	70

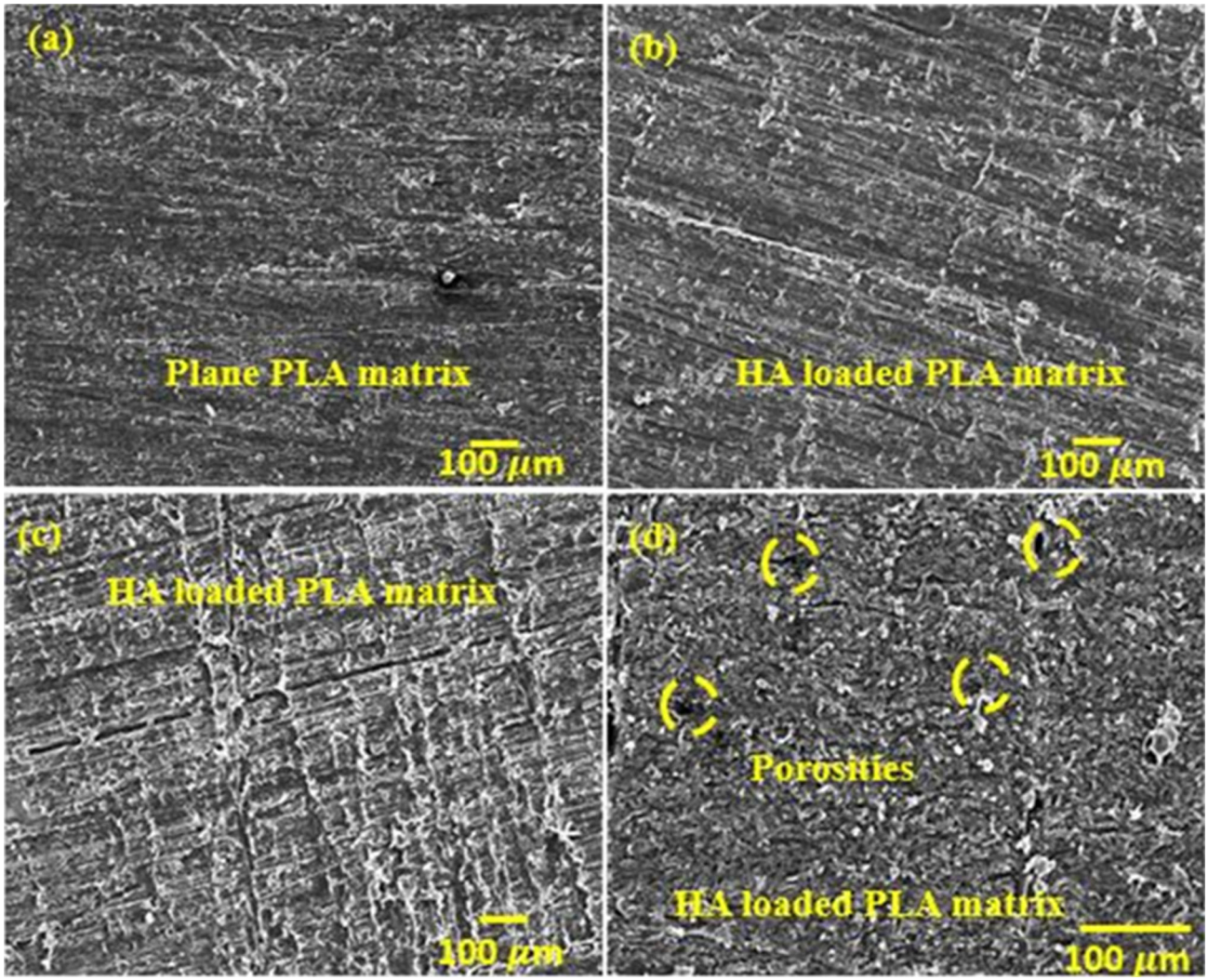

Fig. 2 Surface morphology of as-printed specimens: (a) pure PLA, (b) PLA with 4 wt.% HA, (c) PLA with 6 wt.% of HA, and (d) PLA with 8 wt.% of HA (printed at 100% infill density)

(SEM; make: Zeiss EVO 50) has been used. The effect of shape recovery was also studied on the sample by provided load till the elastic modulus only and later on sample was removed and heated till the annealing temperature.

2.3 Stage 3

In the last stage, based on the best parameter setting, encountered in stage 2, a set of $n = 20$ samples has been printed and thereafter tested in the same manner as discussed in stage 2 for mechanical characteristics. Further, *Weibull* analysis is utilized to determine the reliability of 3D printed scaffolds. The *Weibull* modulus (β) measures the strength reliability of 3D printed scaffolds and a minimum of 20 readings for each output response characteristic has been recorded for the statistical analysis.

The probability of failure, P_f represents the reliability of 3D printed scaffolds and can be computed according to as below equation (Ref 46-48):

$$P_f(\sigma) = 1 - \exp\left[-\left(\frac{\sigma - \sigma_t}{\sigma_o}\right)^{\mu}\right], \sigma \geq 0, \mu \geq 0, \sigma_o \geq 0 \quad \text{(Eq 2)}$$

where σ is the characteristics (FS/CS) at failure, σ_o is the scale parameters, σ_t is the threshold value of characteristics below which probability of failure is zero (set to zero), and μ is the

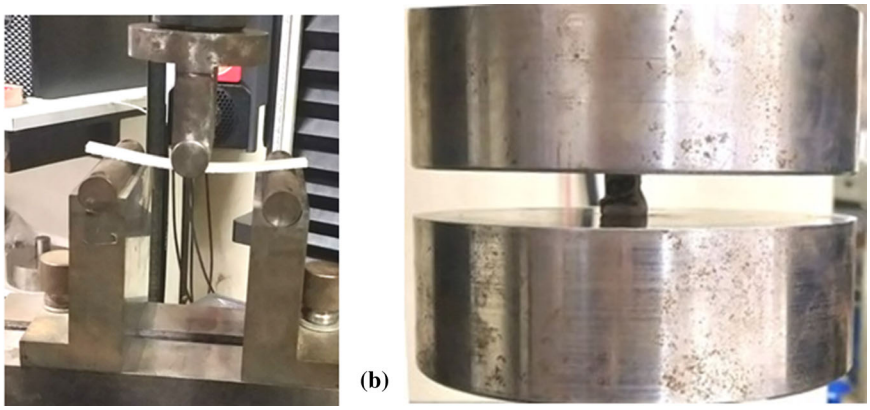

Fig. 3 Fixtures and testing of printed samples: (a) flexural and (b) compression

Weibull modulus. This assumption together with uniaxial stress leads to the following expression (3). Where γ is the position parameter, if $\gamma = 0$, the model degrades into two-parameter *Weibull* distribution; η is the scale parameter and β is the shape parameter. The two-parameter *Weibull* distribution can be written as:

$$P_f(\sigma) = 1 - exp\left[-\left(\frac{\sigma}{\sigma_o}\right)^{\mu}\right], \mu \geq 0, \sigma_o \geq 0 \quad \text{(Eq 3)}$$

After taking the natural logarithm of both sides of the Eq. (2) is taken, the Eq. (4) can be written:

$$\ln\left[\ln\left(\frac{1}{1 - P_f(\sigma)}\right)\right] = \mu \times \frac{\sigma}{\sigma_o} \quad \text{(Eq 4)}$$

The probability of $F(x)$ was computed by Bernard's Median Rank formula, as represented in Eq. (5):

$$F(x) = \frac{i - 0.5}{N} \quad \text{(Eq 5)}$$

where i is the serial number of the output response characteristics and N is the total test number of samples.

2.4 Stage 4

The bioactivity of 3D printed scaffolds was accessed using in vitro analysis using bone marrow mesenchymal stem cells (BMSCs) cell line. The BMSCs cell lines were derived from the Sprague–Dawley rat model. The effect of HA concentration on cell proliferation and differentiation (MTT assay, DNA content, and ALP activity) on 3D printed scaffolds samples. The cells were cultured in αMEM supplemented with 10% FBS, 100 IU/mL penicillin (Sigma Inc.), and 100 mg/mL streptomycin (Sigma) in an incubator (Sanyo, Japan) with 5% CO_2 supply at 37 °C and saturated humidity.

Confluent cells were seeded on the scaffold samples and growth of cells was recorded for a predetermined time of 1, 3, and 7 days. The visual examination of cell attachment and growth was investigated by Olympus microscope. Moreover, cell growth in terms of cell number counts was recorded using hemo-cytometer (Ref 49, 50). The yellow dye 3-(4,5-dimethylthiazol-2-yl)-2,5-diphenyltetrazolium bromide was used to access the cell viability and proliferation. The MTT dye superimposes the nucleus of live cells and produces insoluble purple formazan crystals. The results of the MTT assay were recorded in terms of optical density at 570 nm wavelength. The cell differentiation in terms of alkaline phosphatase-specific (ALP) activity was investigated. Three samples were used in each group by reporting the results as mean ± standard deviation. One-way analysis of variance (ANOVA) was performed considering $p < 0.05$ statistically significant. The cell adhesion on the samples was observed under the scanning electron microscopy (SEM, Zeiss, Germany) after the fixation, while the cell fixation was carried out according to the protocol reported (Ref 51-53).

3. Results and Discussion

3.1 Effect of Input Parameters on Mechanical Properties

Figures 4 and 5 show the stress–strain curve and fractured micrograph of the fabricated 3D printed scaffolds under flexural and compressive loading, respectively. It can be seen in Fig. 4(a) that with an increase in the wt.% of HA loading in the PLA matrix, the FS of the 3D printed composite scaffolds decreased and also the flexural modulus decreases from 3600 to ∼ 2000 MPa. The main reason behind this trend is mainly because of the lack of physical bonding between the HA particles and the PLA matrix. And due to the poor compatibility of the PLA matrix with HA particles, the resulted FS reduced, significantly. As observed, the maximum level of FS and flexural modulus obtained in the present case ranged ∼100 MPa and ∼ 3600 MPa, with 4 wt.% of HA particles, which is 65% and 55.55% more when compared to the scaffold prepared with 8 wt.% of HA particle loading.

Further, Fig. 4(d) shows that the surface of the fractured specimen with 4 wt.% of HA particles resulted in the ductile fracture as a clear indication of fiber pulling and elongation has been appeared. In the case of Fig. 4b), it has been seen that the maximum FS (∼ 113 MPa) and Flexural modulus (∼ 3459 MPa) is obtained for the scaffolds prepared at 100% infill density. This is mainly because of the structural soundness of the scaffold that resulted due to the higher level of infill density. When compared to the 20% infill density, the FS obtained with 100% infill density is 4.52 times higher. The fractured surface, refer Fig. 4(e), as captured for the specimen prepared with 100% infill density, indicated brittle fracture. The layer of the scaffold which is having a 20% infill percentage is ruptured by crossing the adjacent layers and fiber elongations. As regard the annealing temperature, it has been found in the

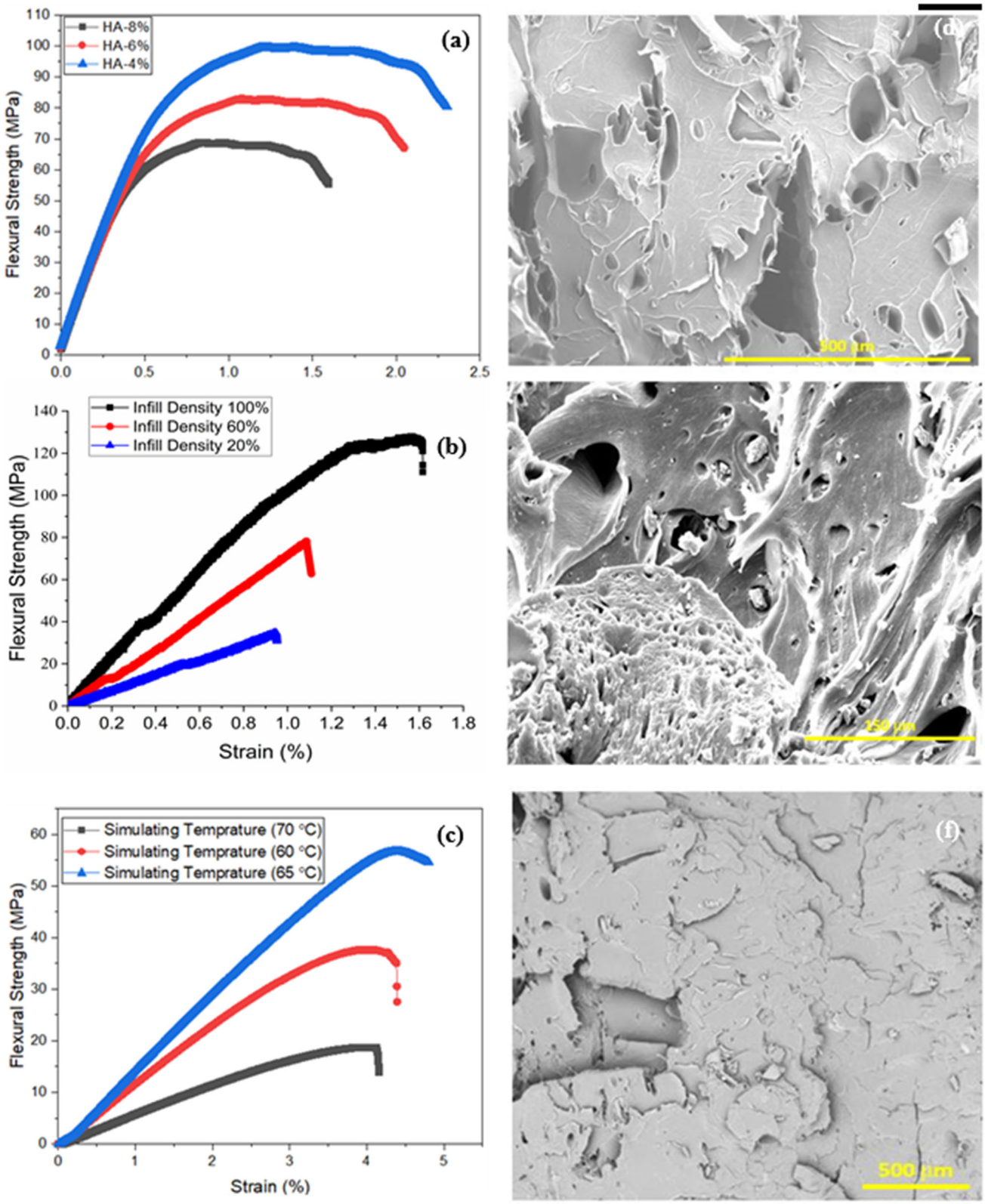

Fig. 4 FS curves: (a) effect of wt.% of HA loading in PLA matrix (samples printed at 20% infill density), (b) effect of infill density (samples printed with 4 wt.% of HA), (c) effect of annealing temperature (printed with 4 wt.% of HA and 20% infill density), and (d–f) morphology of the respected fractured scaffolds

case of Fig. 4(c) that the FS and flexural modulus of the scaffolds decreased by increasing the temperature from 60 to 65 °C. The annealing temperature, at 65 °C, provided an adequate fusion between layers that led to the most resistive combination for bending deformation.

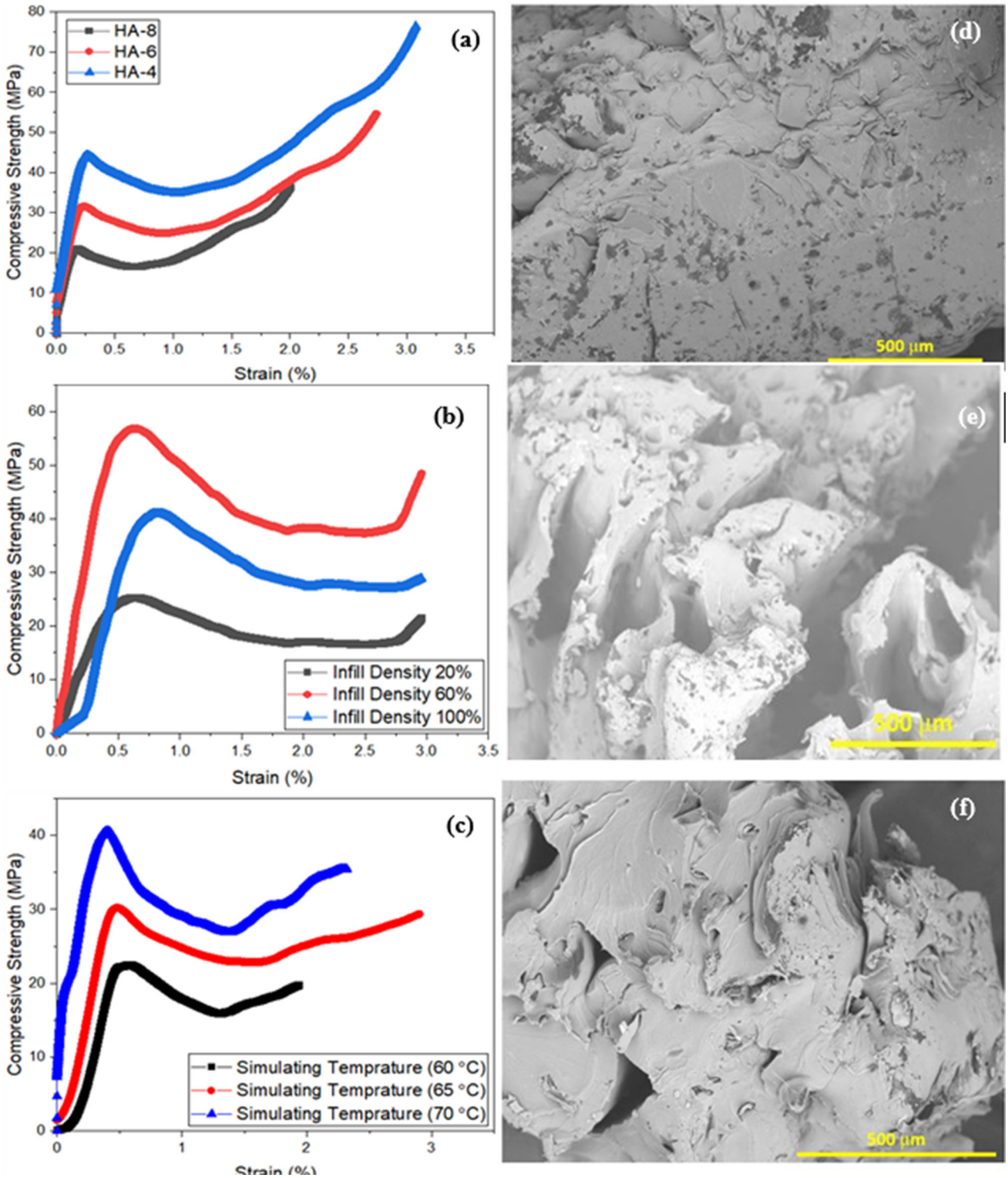

Fig. 5 CS curves: (a) effect of wt.% of HA loading in PLA matrix (samples printed at 60% infill density), (b) effect of infill density (samples printed with 4 wt.% of HA), (c) effect of annealing temperature (printed with 4 wt.% of HA and 60% infill density), and (d–f) morphology of the respected fractured scaffolds

However, a further increase in the annealing temperature, to 70 °C, dropped the FS. In this case, the maximum FS and flexural modulus were recorded of 56 MPa and 1500 MPa. From Fig. 4(f), it can be seen that limited fiber elongation took place upon external loading. In the case of FS, the best printing parametric level, as observed, are 4% wt. loading of HA particles, 100% infill density, and 65 °C annealing temperature. The results of CS are given in Fig. 5. It can be seen in Fig. 5(a) that the CS of the developed scaffolds decreased by increasing the wt.% of HA particles in the PLA matrix. The reason behind

the trend, being similar to FS, is due to the presence of the large amount HA ceramic particles in the polymeric chain of PLA that resulted in discontinuities in the regular PLA's polymer chain. This resulted in an easy dislocation of the chain upon loading. However, compared to the loading levels of HA loadings, the specimen prepared with 4 wt.% of HA particles survived and obtained maximum CS of ~76 MPa and compression modulus of 3900 MPa. Ductile fracture morphology, identified in Fig. 5(d), indicated that the PLA fibers elongated to a great extent before presenting a fracture.

In the case of Fig. 5(b), it has been found that the maximum CS and compression modulus has been recorded in for the scaffolds prepared at 60% infill, followed by 100% infill density. The morphology of the fractured surface, in case of maximum CS, indicated the presence of combined ductile–brittle fracture, refer Fig. 5(e). Finally, refer to Fig. 5(c), it has been found that the CS of the specimens increased by increasing the annealing temperature, with maximum strength recorded of 41.5 MPa in case of 70 °C annealing temperature. The exposure of printed scaffolds to 70 °C annealing temperature increased the brittleness of the same, as seen in Fig. 5(f).

Also the shape recovery of the samples with respect to HA loading, infill density and simulating temperature was studied. It was observed that the shape recovery percentage was increased from ~ 82.87 to ~ 85.89% with increasing the HA loading from 4 to 8%. It could be due to the shape recovery nature of HA which acted as a nuclie in the PLA. However, the improvement in shape recovery with respect to HA laoding was not significant. The higher infill density in the PLA scaffolds results in higher value of ~ 92.14% shape recovery percentage. It was due to better moduls of the 100% infill density as compare to 20% infill density. The annealing temperature of 60, 65 an 70 °C also contributed ~ 71.8, ~ 73.5 and ~ 77.8% of shape recovery after unloading the force. After analyzing the effect of HA loading, infill density and annealing temperature, the optimized parameters were finalized. These are 4% wt. loading of HA particles, 100% infill density, and 65 °C annealing temperature. Further experiments were performed on these parameters for Weibull analysis.

3.2 Weibull Analysis Outcomes

To validate the predicted results, confirmation experiments were performed for each output response characteristics and very high fluctuations in the mean of the obtained readings have been identified. So, to test the reliability of the findings, an attempt has been made using *Weibull* distribution analysis. For the optimized setting of each out response characteristic of as-fabricated component, 20 confirmation tests were conducted.

It has been observed that the observed values were different with error ranging from 5-10% from the predicted value at optimized setting. Therefore, *Weibull*-statistical analysis is used to estimate the variability of 3D printed scaffolds. Figure 6 shows the Weibull probability, $P_f(\sigma)$ plot of each group for FS and CS, and various *Weibull* parameters such as scale (σ_o) and modulus (μ) were calculated for each out response characteristics of the as-fabricated component. A linear pattern was established and the co-efficient of determination (R^2) for FS and CS was calculated as 0.96 and 0.98, respectively, which shows the strong relationship between the experimental value and fitted curve. The FS of 3D printed scaffolds was observed during the confirmation tests was in the range of 110.12 MPa to 125.99 GPa. The deviation between predicted and observed

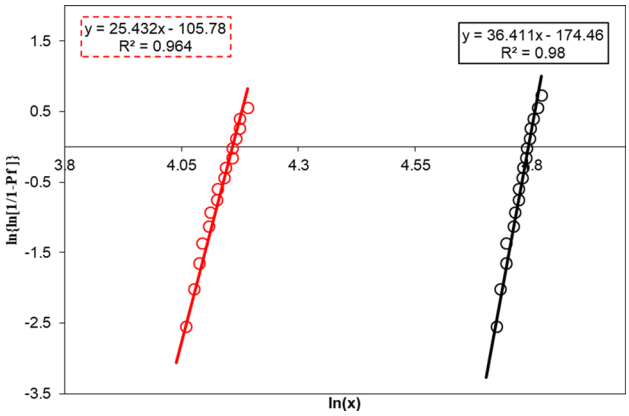

Fig. 6 *Weibull* distribution for FS (red color) and CS (black color) of the 3D Printed PLA/HA scaffolds

values is 11.87%. The *Weibull* modulus was used to determine the failure probability of components (Ref 54, 55). The *Weibull* modulus for FS of 3D printed scaffolds was 36.41. The probability of failure of 3D printed scaffolds under flexural load is low and reliability is not compromised, which conferred that the PLA/HA is potential materials for scaffold applications.

The CS of 3D printed scaffolds was observed during the confirmation tests was in the range of 56.78–69.99 MPa. The deviation between predicted and observed values is 16.35%. The *Weibull* modulus for FS of 3D printed scaffolds was 25.43.

The probability of failure of 3D printed scaffolds under compressive load is low and reliability is not compromised, which conferred that the PLA/HA is potential materials for scaffold applications. The above interpretation revealed that the reliability of the mechanical properties of the 3D printed scaffolds can be analyzed and represented by the two parameters *Weibull's* distribution. The mean value of the output put characteristics (FS and CS) is calculated by Eq. (6):

$$\int_0^\infty R_t \mathrm{d}t = \gamma + \eta \times \Gamma\left(\frac{1}{\mu} + 1\right), \gamma = 0 \qquad \text{(Eq 6)}$$

where Γ is the gamma function.

After putting values of η and μ into the formula (6), the mean value of the FS and CS was obtained as 118.67 MPa and 62.12MPA, respectively. The predicted values of FS and CS by *Weibull* analysis are very close to the experimental values. The deviation is less than 5% in all the cases, which indicated the precision is high from the perspective of reliability design, so using the two parameters *Weibull* distribution analysis was successfully used to express the reliability of the mechanical properties of the as-fabricated component is reasonable.

3.3 In Vitro Bioactivity Analysis

Figure 7 shows the cell growth, proliferation, differentiation, and cell attachment on the 3D printed scaffolds. Figure 7(a–c) shows the effect on HA concentration on cell proliferation and differentiation (MTT assay, DNA content, and ALP activity) of BMSCs cells on Days 1, 3, and 7 after seeding on scaffold samples. All observed data were statically analyzed at a 95% confidence level using ANOVA, and the individual group was statistically highly significant ($p < 0.001$) for each treatment (different HA compositions) at different time intervals (days). Figure 7(a) shows the cell proliferation activities

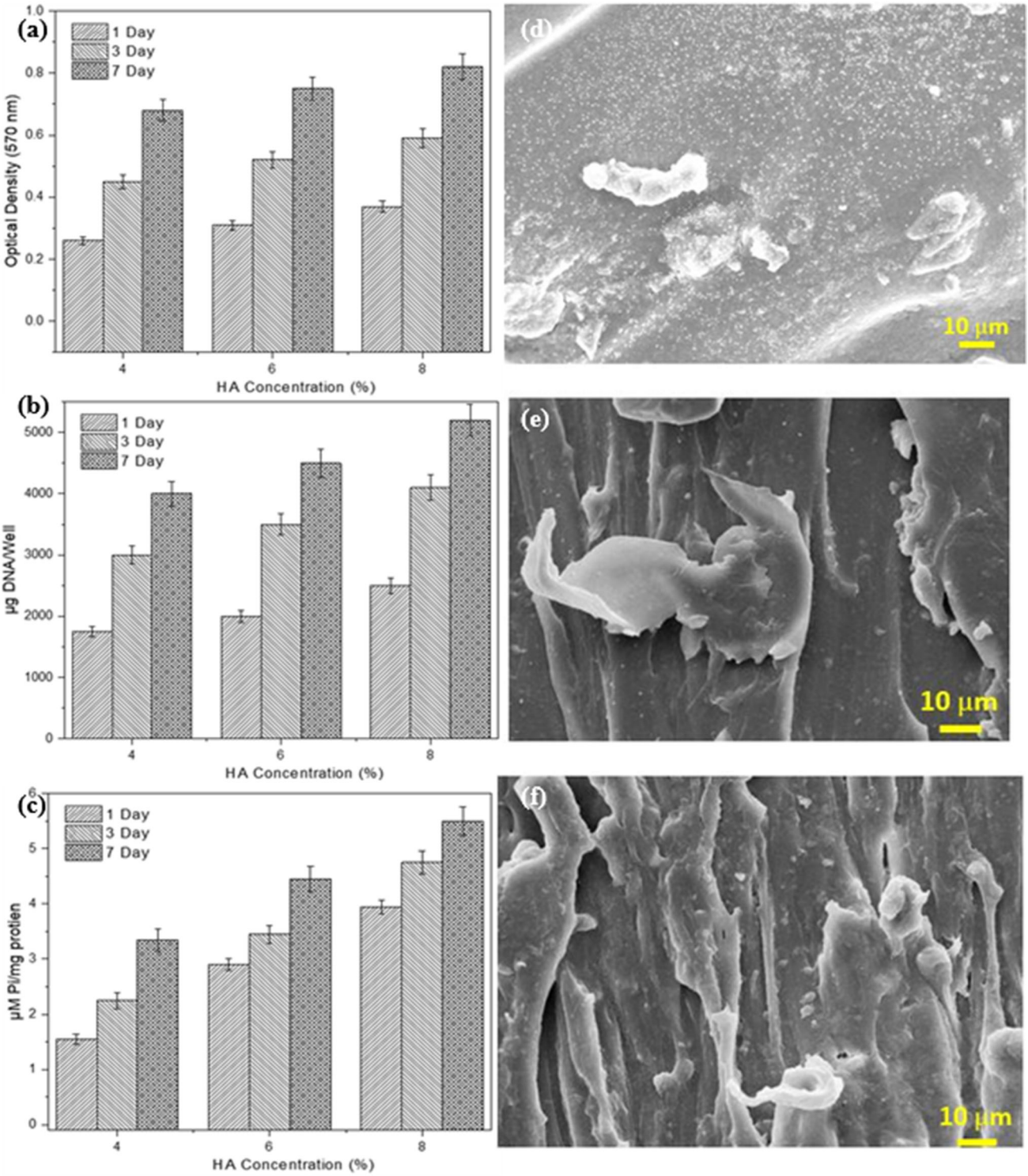

Fig. 7 Effect of HA on cell proliferation and differentiation of BMSCs cells determined on day 1st, 3rd, and 7th after seeding on 3D printed Scaffolds (a) MTT assay, (b) DNA content, and (c) ALP activity; SEM micrograph of cell attachments on PLA/HA scaffolds (d-f)

for 1, 3, and 7 days and it can be seen that the cell growth increased with HA concentration. This was observed because HA promotes the apatite formation and many biological activities such as cytoplasmic extensions, the accusation of filopodia and retraction of an extracellular matrix (ECM) were observed on the samples. Figure 7(b) shows the DNA content activity on the scaffold samples at different HA concentration and it was observed that DNA content increased with HA concentration. This is because the higher HA concentration escalated the surface energy, which promoted protein absorption and results in increased DNA content. Figure 7(c) shows the ALP-type differentiation activities on the scaffold samples at different HA concentration. Owing to presence to HA in the PLA matrix, various biological activities like extracellular

matrix (ECM), and filopodia were initiated, which are the complete sign of differentiation activities. Due to differences in the biological characteristics of HA particles and PLA, an insignificant reaction occurred for the modification of the surface properties. However, the composite scaffolds with a higher level of the infill density are generally recommended for the load-bearing implant applications (Ref 42). In the case of tissue engineering applications, scaffolds should be having low infill density for the tissue growth with strong grip strength by porous channels (Ref 43). So, the effect of 20% infill density in case of 4%, 6%, and 8% wt. of HA loading was studied.

The combined effect of HA cell adhesion nature and designed porous architecture shown the most significant cell proliferation in PLA/HA at 8 wt.% of HA with 20% infill density. The positive effect of HA wt.% was observed on the biocompatibility study of the 3D printed composite scaffolds. Cell adhesion study was performed with BMSCs cell lines for 1, 3, and 7 days. Figure 7(d–f) shows the attached cell morphology on the scaffolds surface at 4%, 6%, and 8% concentration of HA in PLA. Various biological activities such as cytoplasmic extensions, redirection of extracellular matrix (ECM), and filopodia accusation were observed, which indicates that the cell grown on all scaffolds specimens' surfaces. The scaffold surface is non-toxic and hydrophilic, which promotes cell attachment and growth. The filopodia (yellow arrows) being extended by some of the growing cells on the surface of the scaffold can be seen from the SEM micrograph. Moreover, variation in the cell growth pattern also potentially suggests osteoconductive characteristics of cells. Higher cell attachment was observed on the scaffolds with HA 8 wt.%, as can be seen in Fig. 7(f).

This is because, at 8% HA concentration, the porous architecture of the fabricated specimens catalyzed the proliferation of cells, homogenous rearrange, and attached to the surface (Ref 41). Moreover, it was also attributed due to enough change in surface tension and hydrophilic nature of the surface of the composite as discussed above.

4. Conclusions

Based on the conclusions drawn in the present study, the following conclusions have been drawn:

- It has been found that the fabricating parameters, such as wt.% of HA particles, infill density, and annealing temperature, have influenced the FS and CS of the developed scaffoldings to a great extent. Although, the parameter, wt.% of HA particles, has increased the cell adhesion, growth, and proliferation in a linear order, however, an increase in the same did not show a positive effect on mechanical characteristics, both FS and CS. Further, in the case of infill density, it has been found that the maximum FS and CS corresponded to 100% and 60% infill density, respectively. Lastly, the results of the annealing temperature indicated that the maximum FS and CS have been obtained at 65 °C and 70 °C, respectively.
- The *Weibull* analysis, for mechanical reliability, of the developed PLA/HA scaffolds revealed that the strength reliability has not been compromised. A linear pattern was established and the co-efficient of determination (R^2) for FS and CS was calculated as 0.96 and 0.98, respectively, indicated a strong relationship between the experimental value and fitted curve. The deviation recorded was less than 5% for FS and CS, indicated the precision is high from the perspective of reliability design.
- PLA/HA exhibited excellent biocompatibility and bioactivity. Bioactivity analysis showed the significant effect of HA concentration and infill density was observed on the wettability and biocompatibility study. The PLA/HA scaffold with 8 wt.% of HA particles and 20% infill density resulted in the most dominating hydrophilic nature along with strong adhesive cell compatibility.
- This study provides an insight into the application of PLA/HA scaffold as shape memory composite expect that the materials will be very useful for potential tissue engineering and biomedical applications.

References

1. Y. Guo, Z. Lv, Y. Huo, L. Sun, S. Chen, Z. Liu, C. He, X. Bi, X. Fan, and Z. You, A Biodegradable Functional Water-Responsive Shape Memory Polymer for Biomedical Applications, *J. Mater. Chem. B*, 2019, **7**(1), p 123–132
2. S. Singh, G. Singh, C. Prakash, S. Ramakrishna, L. Lamberti, and C. Pruncu, 3D Printed Biodegradable Composites: An Insight into Mechanical Properties of PLA/Chitosan Scaffold, *Polym. Test.*, 2020, **89**, p 106722
3. X. Xiao, X. Huang, F. Ye, B. Chen, C. Song, J. Wen, Z. Zhang, G. Zheng, H. Tang, and X. Xie, The miR-34a-LDHA Axis Regulates Glucose Metabolism and Tumor Growth in Breast Cancer, *Sci. Rep.* 2016, 6
4. Z.Q. Liu, D. Jiao, and Z.F. Zhang, Remarkable shape memory effect of a natural biopolymer in aqueous environment, *Biomaterials*, 2015, **65**, p 13–21
5. F. Ji, J. Li, Y. Weng, and J. Ren, Synthesis of PLA-Based Thermoplastic Elastomer and Study on Preparation and Properties of PLA-Based Shape Memory Polymers, *Mater. Res. Express*, 2019, **7**(1), p 015315
6. R. Tejero, E. Anitua, and G. Orive, Toward the Biomimetic Implant Surface, Biopolymers on Titanium-Based Implants for Bone Regeneration, *Prog. Polym. Sci.*, 2014, **39**, p 1406–1447
7. S. Wu, X. Liu, K.W. Yeung, C. Liu, and X. Yang, Biomimetic Porous Scaffolds for Bone Tissue Engineering, *Mater. Sci. Eng. R Rep.*, 2014, **80**, p 1–36
8. G.J.M. Antony, S.T. Aruna, and S. Raja, Enhanced Mechanical Properties of Acrylate Based Shape Memory Polymer Using Grafted Hydroxyapatite, *J. Polym. Res.*, 2018, **25**(5), p 120
9. H. Kalita, *Shape Memory Polymers, Theory and Application*, Walter de Gruyter GmbH & Co KG, Berlin, 2018
10. J. Wang, Q. Zhao, H. Cui, Y. Wang, H. Chen, and X. Du, Tunable Shape Memory Polymer Mold for Multiple Microarray Replications, *J. Mater. Chem. A*, 2018, **6**(48), p 24748–24755
11. R.U. Hassan, S. Jo, and J. Seok, Thermorheological Characteristics and Comparison of Shape Memory Polymers Fabricated by Novel 3D Printing Technique, *Funct. Mater. Lett.*, 2018, **11**(02), p 365
12. S. Jose, J. J. George, S., Siengchin, and J. Parameswaranpillai, Introduction to Shape Memory Polymers, Polymer Blends and Composites, State of the Art, Opportunities, New Challenges and Future Outlook. In *Shape Memory Polymers, Blends and Composites* 2020 (pp. 1–19). Springer, Singapore
13. C. Rosales, H. Kim, M. Duarte, L. Chavez, T. Tseng, and Y. Lin, Toughness-Based Recovery Efficiency of Shape Memory Parts Fabricated Using Material Extrusion 3D Printing Technique, *Rapid Prototyp. J.*, 2019, **25**, p 30–37
14. G. Kim, S. Lee, H. Kim, D. Yang, Y. Kim, Y. Kyung, Y. Kim, C. Choi, S. Kim, and S. Kwon, Three-Dimensional Printing, Basic Principles and Applications in Medicine and Radiology, *Kor. J. Radiol.*, 2016, **17**(2), p 182–197

15. A. Bandyopadhyay, S. Bose, and S. Das, 3D Printing of Biomaterials, *MRS Bull.*, 2015, **40**(2), p 108–115
16. C. O'Brien, B. Holmes, S. Faucett, and L. Zhang, Three-Dimensional Printing of Nanomaterial Scaffolds for Complex Tissue Regeneration, *Tissue Eng. Part B Rev.*, 2014, **21**(1), p 103–114
17. F. Senatov, K. Niaza, M. Zadorozhnyy, A. Maksimkin, S. Kaloshkin, and Y. Estrin, Mechanical Properties and Shape Memory Effect of 3D-Printed PLA-Based Porous Scaffolds, *J. Mech. Behav. Biomed. Mater.*, 2016, **57**, p 139–148
18. F. Senatov, M. Zadorozhnyy, K. Niaza, V. Medvedev, S. Kaloshkin, N. Anisimova, M. Kiselevskiy, and K. Yang, Shape Memory Effect in 3D-Printed Scaffolds for Self-Fitting Implants, *Eur. Polym. J.*, 2017, **93**, p 22–31
19. Y. Choong, S. Maleksaeedi, H. Eng, J. Wei, and P. Su, 4D Printing of High Performance Shape Memory Polymer Using Stereolithography, *Mater. Des.*, 2017, **15**, p 219–225
20. J. Wu, C. Yuan, Z. Ding, M. Isakov, Y. Mao, T. Wang, M. Dunn, and H. Qi, Multi-shape Active Composites by 3D Printing of Digital Shape Memory Polymers, *Sci. Rep.* 2016, 13
21. Y. Yang, Y. Chen, Y. Wei, and Y. Li, 3D Printing of Shape Memory Polymer for Functional Part Fabrication, *Int. J. Adv. Manuf. Technol.*, 2016, **84**(9), p 2079–2095
22. Q. Zhang, K. Zhang, and G. Hu, Smart Three-Dimensional Lightweight Structure Triggered from a Thin Composite Sheet via 3D Printing Technique, *Sci. Rep.*, 2016, **29**(6), p 22431
23. R. Matsuzaki, M. Ueda, M. Namiki, T. Jeong, H. Asahara, K. Horiguchi, T. Nakamura, A. Todoroki, and Y. Hirano, Three-Dimensional Printing of Continuous-Fiber Composites by In-Nozzle Impregnation, *Sci. Rep.*, 2016, **6**, p 1–7
24. S. Chen, Q. Zhang, and J. Feng, 3D Printing of Tunable Shape Memory Polymer Blends, *J. Mater. Chem. C*, 2017, **5**(33), p 8361–8365
25. C. Garcia Rosales, H. Kim, M. Garcia, L. Chavez, M. Castañeda, T. Tseng, and Y. Lin, Characterization of Shape Memory Polymer Parts Fabricated Using Material Extrusion 3D Printing Technique, *Rapid Prototyp. J.*, 2019, **25**(2), p 322–331
26. I. Garces, S. Aslanzadeh, Y. Boluk, and C. Ayranci, Effect of Moisture on Shape Memory Polyurethane Polymers for Extrusion-Based Additive Manufacturing, *Materials*, 2019, **12**(2), p 244
27. H. Wu, P. Chen, C. Yan, C. Cai, and Y. Shi, Four-Dimensional Printing of a Novel Acrylate-Based Shape Memory Polymer Using Digital Light Processing, *Mater. Des.*, 2019, **171**, p 107704
28. T. Zhao, R. Yu, X. Li, B. Cheng, Y. Zhang, X. Yang, X. Zhao, Y. Zhao, and W. Huang, 4D Printing of Shape Memory Polyurethane via Stereolithography, *Eur. Polym. J.*, 2018, **101**, p 120–126
29. R. Yu, X. Yang, Y. Zhang, X. Zhao, X. Wu, T. Zhao, Y. Zhao, and W. Huang, Three-Dimensional Printing of Shape Memory Composites with Epoxy-Acrylate Hybrid Photopolymer, *ACS Appl. Mater. Interfaces*, 2017, **9**(2), p 1820–1829
30. Y. Choong, S. Maleksaeedi, H. Eng, P. Su, and J. Wei, Curing Characteristics of Shape Memory Polymers in 3D Projection and Laser Stereolithography, *Virt. Phys. Prototyp.*, 2017, **12**(1), p 77–84
31. C. Yuan, D. Roach, C. Dunn, Q. Mu, X. Kuang, C. Yakacki, T. Wang, K. Yu, and H. Qi, 3D Printed Reversible Shape Changing Soft Actuators Assisted by Liquid Crystal Elastomers, *Soft Matter*, 2017, **13**(33), p 5558–5568
32. M. Bodaghi, A. Damanpack, and W. Liao, Triple Shape Memory Polymers by 4D Printing, *Smart Mater. Struct.*, 2018, **27**(6), p 065010
33. S. Singh, G. Singh, C. Prakash, and S. Ramakrishna, Current Status and Future Directions of Fused Filament Fabrication, *J. Manuf. Process.*, 2020, **55**, p 288–306
34. Z. Zhao, F. Peng, K. Cavicchi, M. Cakmak, R. Weiss, and B. Vogt, Three-Dimensional Printed Shape Memory Objects Based on an Olefin Ionomer of Zinc-Neutralized Poly (Ethylene-co-methacrylic Acid), *ACS Appl. Mater. Interfaces*, 2017, **9**(32), p 27239–27249
35. M. Kang, Y. Pyo, J. Jang, Y. Park, Y. Son, M. Choi, J. Ha, Y. Chang, and C. Lee, Design of a Shape Memory Composite (SMC) Using 4D Printing Technology, *Sens. Actuators A*, 2018, **283**, p 187–195
36. W. Wu, W. Ye, Z. Wu, P. Geng, Y. Wang, and J. Zhao, Influence of Layer Thickness, Raster Angle, Deformation Temperature and Recovery Temperature on the Shape-Memory Effect of 3D-Printed Polylactic Acid Samples, *Materials*, 2017, **10**(8), p 970
37. G. Hu, A. Damanpack, M. Bodaghi, and W. Liao, Increasing Dimension of Structures by 4D Printing Shape Memory Polymers via Fused Deposition Modeling, *Smart Mater. Struct.*, 2017, **26**(12), p 125023
38. X. Peng, H. He, Y. Jia, H. Liu, Y. Geng, B. Huang, and L. Luo, Shape Memory Effect of Three-Dimensional Printed Products Based on Polypropylene/Nylon 6 Alloy, *J. Mater. Sci.*, 2019, **54**(12), p 9235–9246
39. A. Farzadi, V. Waran, M. Solati-Hashjin, Z. Rahman, M. Asadi, and N. Osman, Effect of Layer Printing Delay on Mechanical Properties and Dimensional Accuracy of 3D Printed Porous Prototypes in Bone Tissue Engineering, *Ceram. Int.*, 2015, **41**(7), p 8320–8330
40. M. Castilho, M. Dias, U. Gbureck, J. Groll, P. Fernandes, I. Pires, B. Gouveia, J. Rodrigues, and E. Vorndran, Fabrication of Computationally Designed Scaffolds by Low Temperature 3D Printing, *Biofabrication*, 2013, **5**(3), p 035012
41. M. Castilho, J. Rodrigues, I. Pires, B. Gouveia, M. Pereira, C. Moseke, J. Groll, A. Ewald, and E. Vorndran, Fabrication of Individual Alginate-TCP Scaffolds for Bone Tissue Engineering by Means of Powder Printing, *Biofabrication*, 2015, **7**(1), p 015004
42. S. Meininger, S. Mandal, A. Kumar, J. Groll, B. Basu, and U. Gbureck, Strength Reliability and In Vitro Degradation of Three-Dimensional Powder Printed Strontium-Substituted Magnesium Phosphate Scaffolds, *Acta Biomater.*, 2016, **31**, p 401–411
43. M. Castilho, M. Dias, E. Vorndran, U. Gbureck, P. Fernandes, I. Pires, B. Gouveia, H. Armés, E. Pires, and J. Rodrigues, Application of a 3D Printed Customized Implant for Canine Cruciate Ligament Treatment by Tibial Tuberosity Advancement, *Biofabrication*, 2014, **6**(2), p 025005
44. Y. Lu, Z. Mei, J. Zhang, S. Gao, X. Yang, B. Dong, L. Yue, and H. Yu, Flexural Strength and Weibull Analysis of Y-TZP Fabricated by Stereolithographic Additive Manufacturing and Subtractive Manufacturing, *J. Eur. Ceram. Soc.*, 2020, **40**(3), p 826–834
45. M. Castilho, B. Gouveia, I. Pires, J. Rodrigues, and M. Pereira, The Role of Shell/Core Saturation Level on the Accuracy and Mechanical Characteristics of Porous Calcium Phosphate Models Produced by 3D Printing, *Rapid Prototyp. J.*, 2018, **21**, p 43–55
46. K. Naresh, K. Shankar, and R. Velmurugan, Reliability Analysis of Tensile Strengths Using Weibull Distribution in Glass/Epoxy and Carbon/Epoxy Composites, *Compos. B Eng.*, 2018, **133**, p 129–144
47. Ö. Keleş, C. Blevins, and K. Bowman, Effect of Build Orientation on the Mechanical Reliability of 3D Printed ABS, *Rapid Prototyp. J.*, 2017, **23**, p 320–328
48. Z. An, T. Chen, D. Cheng, T. Chen, and Z. Wang, Statistical Analysis and Prediction on Tensile Strength of 316L-SS Joints at High Temperature Based on Weibull Distribution, *IOP Conf. Ser. Mater. Sci. Eng.*, 2017, **281**, p 012062
49. C. Prakash, S. Singh, S. Ramakrishna, G. Królczyk, and C. Le, Microwave Sintering of Porous Ti–Nb–HA Composite with High Strength and Enhanced Bioactivity for Implant Applications, *J. Alloys Compd.*, 2020, **824**, p 153774
50. C. Prakash, and S. Singh, On the Characterization of Functionally Graded Biomaterial Primed Through a Novel Plaster Mold Casting Process, *Mater. Sci. Eng. C* (2020), p 110654
51. G. Singh, S. Singh, C. Prakash, R. Kumar, R. Kumar, and S. Ramakrishna, Characterization of Three-Dimensional Printed Thermal-Stimulus Polylactic Acid-Hydroxyapatite-Based Shape Memory Scaffolds, *Polym. Compos.*, 2020, **41**(9), p 3871–3891
52. A. Pandey, G. Singh, S. Singh, K. Jha, and C. Prakash, 3D Printed Biodegradable Functional Temperature-Stimuli Shape Memory Polymer for Customized Scaffoldings, *J. Mech. Behav. Biomed. Mater.*, 2020, **108**, p 103781
53. C. Prakash, S. Singh, M. Singh, K. Verma, B. Chaudhary, and S. Singh, Multi-Objective Particle Swarm Optimization of EDM Parameters to Deposit HA-Coating on Biodegradable Mg-Alloy, *Vacuum*, 2018, **158**, p 180–190
54. C. Griffiths, J. Howarth, G. De Almeida-Rowbotham, A. Rees, and R. Kerton, A Design of Experiments Approach for the Optimisation of Energy and Waste During the Production of Parts Manufactured by 3D Printing, *J. Clean. Prod.*, 2016, **139**, p 74–85
55. B. Basu, D. Tiwari, D. Kundu, and R. Prasad, Is Weibull Distribution the Most Appropriate Statistical Strength Distribution for Brittle Materials?, *Ceram. Int.*, 2009, **35**, p 237–246